analytical chemistry

Article

pubs.acs.org/ac



# Real Time Observation of X-ray-Induced Surface Modification Using Simultaneous XANES and XEOL-XANES

Annemie Adriaens,[†] Paul Quinn,[‡] Sergey Nikitenko,[§] and Mark G. Dowsett*[,∥]

[†]Department of Analytical Chemistry, Ghent University, Krijgslaan 281 S12, B9000, Ghent, Belgium

[‡]Diamond Light Source Ltd., Harwell Science and Innovation Campus, Chilton, Didcot OX11 ODE, U.K.

[§]Netherlands Organization for Scientific Research (NWO), DUBBLE@ESRF, BP220, 38043, Cedex 9, France

[∥]Department of Physics, The University of Warwick, Coventry, CV4 7AL, U.K.

**ABSTRACT:** In experiments preliminary to the design of an X-ray-excited optical luminescence (XEOL)-based chemical mapping tool we have used X-ray micro (4.5 × 5.2 $\mu$m) and macro (1 × 6 mm) beams with similar total fluxes to assess the effects of a high flux density beam of X-rays at energies close to an absorption edge on inorganic surfaces in air. The near surface composition of corroded cupreous alloys was analyzed using parallel X-ray and optical photoemission channels to collect X-ray absorption near-edge structure (XANES) data at the Cu K edge. The X-ray fluorescence channel is characteristic of the composition averages over several micrometers into the surface, whereas the optical channel is surface specific to about 200 nm. While the X-ray fluorescence data were mostly insensitive to the X-ray dose, the XEOL-XANES data from the microbeam showed significant dose-dependent changes to the superficial region, including surface cleaning, changes in the oxidation state of the copper, and destruction of surface compounds responsible for pre-edge fluorescence or phosphorescence in the visible. In one case, there was evidence that the lead phase in a bronze had melted. Conversely, data from the macrobeam were stable over several hours. Apart from localized heating effects, the microbeam damage is probably associated with the $O_3$ loading of the surface and increased reaction rate with atmospheric water vapor.

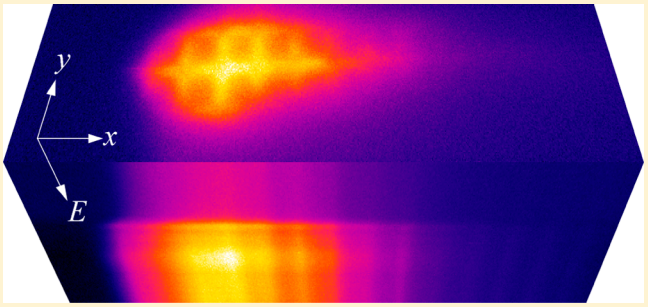


Imaging techniques which can chemically map surfaces in air or a controlled environment (liquid, gas) are few in number. X-ray excited optical luminescence (XEOL)[1−5] is a potentially rich source of information on the chemistry, local atomic order, and electronic structure of a surface. Because the emission concerned lies in the wave bands from the near UV to the near IR, a detector based on more or less conventional light optics can be used.[6,7] This makes the technique capable of mapping in conjunction with either an X-ray microprobe, in which case the detector can be based on a light collection system and a device such as a broadband photomultiplier, or a broader X-ray beam (such as that from a bending magnet) when an imaging detector such as a CCD camera is required. A further attraction of the technique is that, for input X-ray energies from around 3 keV upward, a surface may be observed in air or in a controlled ambient such as a corrosive gas. Under some circumstances, the surface may even be immersed in a liquid,[7,8] although the changes in optical constants induced by radiolysis from the probe complicate the interpretation of the data.[9]

It is well-known that, provided the signal is not swamped by background fluorescence and phosphorescence, the XEOL emission is modulated by the escape probability of a photoelectron at and above an absorption edge. This channel can therefore carry similar X-ray absorption near edge structure (XANES) and extended X-ray absorption fine structure (EXAFS) information to the X-ray fluorescence channel leading to a technique sometimes known as optically detected X-ray absorption spectroscopy (ODXAS). This leads immediately to the possibility of chemical and electronic structure imaging with (at least) micrometer scale lateral resolution.

Our interest in the technique lies in its potential for monitoring surface chemical changes in real time, especially in the context of heritage and other metal corrosion and protection. It is therefore relevant to determine the extent to which the probing X-rays can themselves cause changes in the surface chemistry and to see whether this is related to the total energy absorbed on a pixel during image acquisition or to the energy absorption rate (power), given that, for the same statistical precision in the image, the same number of X-ray photons must be absorbed. Previous studies of damage induced by X-rays in the keV range have shown that both dose and dose rate can be important,[10] that X-ray-induced heating can play a role, for example in the reduction of oxides,[11] and the effects are highly dependent on chemical composition, even in organic thin films.[12] Types of damage are varied, but include reduction,[11] optical damage,[13] hydrocarbon chain breaking, reactions with ozone and other radicals, and thermal[14] and electronic damage.[15] Simultaneous use of XEOL and XANES

**Received:** June 3, 2013
**Accepted:** September 18, 2013
**Published:** September 18, 2013

  

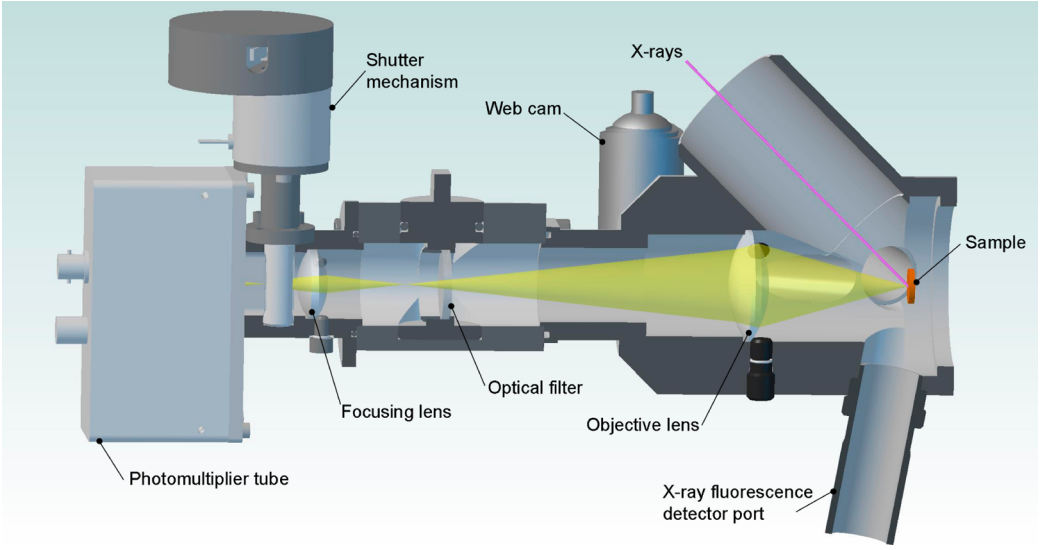


**Figure 1.** Schematic cross section of the light collection system ODXAS1.

or XEOL and X-ray diffraction (XRD) to assess surface damage occurring during analysis seems to be uncommon, but the latter combination has been used in the study of protein crystals.[16]

This work will inform the design process for a XEOL-based microscopy system, in particular the choice between a microprobe device (resolution determined by the X-ray spot size) and a microscope (resolution determined by the light optics and a pixelated detector).

## EXPERIMENTAL SECTION

Microbeam measurements were carried out on a beamline I18[17] at Diamond Light Source (DLS), using a microprobe beam containing a total flux in the range from $10^{11}$ to $10^{12}$ $s^{-1}$. X-rays were incident at 45° to the sample surface, and the illuminated pixel size was 4.5 × 5.2 $\mu$m. The incident angle was chosen to preserve a small beam footprint at high flux density suitable for microprobe imaging. At 9 keV, this gives an input power density of 61.3 W $mm^{-2}$. Copper K-edge XANES spectra were collected on two parallel channels simultaneously: X-ray fluorescence, using a 4-element Vortex ME4 (Hitachi Inc.), and a broadband optical channel from 185 to 850 nm, using a custom detector [optically detected X-ray absorption spectroscope (ODXAS1)] based on fused silica optics and a Hamamatsu 8259-01 broadband photomultiplier tube (see Figure 1).

In what follows, "XANES" will refer to data collected using X-ray fluorescence, and "XEOL-XANES' will be used to describe the parallel optical data. Macrobeam XEOL-XANES measurements were made on a BM26A (DUBBLE)[18] at the ESRF. Again, the X-rays were incident at 45°, and an area 1 × 6 mm was illuminated uniformly. Parallel XANES were not collected. ODXAS1 consists of an uncoated fused silica objective 40 mm in diameter with a 40 mm focal length (Knight Optical LX 4040) and a similar 25 mm diameter demagnifying lens with a 25 mm focal length (Knight Optical LX 2525). Silica is used to avoid secondary fluorescence and to obtain high transmission from the near UV to the near IR, and coatings are avoided to prevent any secondary fluorescence in the optical system. There is a filter carrier for 25 mm diameter optical filters between the two lenses. This was used to filter the emission in the macrobeam experiments. The sample surface is placed 50 mm from the first principal plane of the objective. Since the photomultiplier has no lateral resolution, the optical system is designed to transport as much light as possible into its 4 × 20 mm aperture. The optical axis of ODXAS1 is normal to the sample, and the Vortex detector take-off angle was 10° to the surface (I18 at DLS).

The housing is made from an acetal copolymer, which we have found causes minimal background fluorescence, and a manifold in front of the objective admits X-rays, contains a sample illumination and web-cam-based viewing system, and allows other detectors, such as the Vortex, a view of the sample. A remotely operated fast shutter protects the photomultiplier. The whole device fits onto our electrochemical/environmental cell (eCell),[19] which was used to hold the samples here.

The samples were clean or corroded copper or lead-bronze discs, 12.5 mm in diameter. Copper discs were pressed from 99.9% pure 2 mm thick sheet (Advent), and the lead bronze was an archeological simulant from the IMMACO project.[20] Corroded discs were covered with cuprite ($Cu_2O$), nantokite (CuCl), or a mixture of atacamite and paratacamite [isomeric hydroxychlorides $Cu_2(OH)_3Cl$]. The protocols used to produce the corrosion layers are described in detail elsewhere,[21−23] as are typical XANES data from these samples.[7,8]

The microbeam scan parameters and X-ray flux were chosen to be compatible with the acquisition of XANES and XEOL-XANES spectra from each pixel with acceptable statistics on a practical timescale. For each sample, a sequence of 5 XANES scans across the Cu K edge was taken on the same position. Each scan took 10 min and was divided into two: a pre-edge region from 8.830 to 8.962 keV with a step in monochromator angle of 8.3 mdeg (approximately 5 eV), and a XANES region out to 9.165 keV, sampled at a step of 0.7 mdeg (approximately 0.5 eV). The XANES and XEOL-XANES signals were sampled for 1 s at each step, and the monochromator stepping time was approximately 2 s. The reduction in scan rate at 8.962 keV sometimes leads to significant features in the XEOL-XANES pre-edge signal. These are discussed below. The macrobeam scan parameters were compatible with the acquisition of a microscope image in the XEOL-XANES mode (i.e., the use of a light optical system to collect an image resolved by a pixelated detector rather than a scanned probe), although imaging was


dx.doi.org/10.1021/ac401646q | Anal. Chem. 2013, 85, 9556−9563

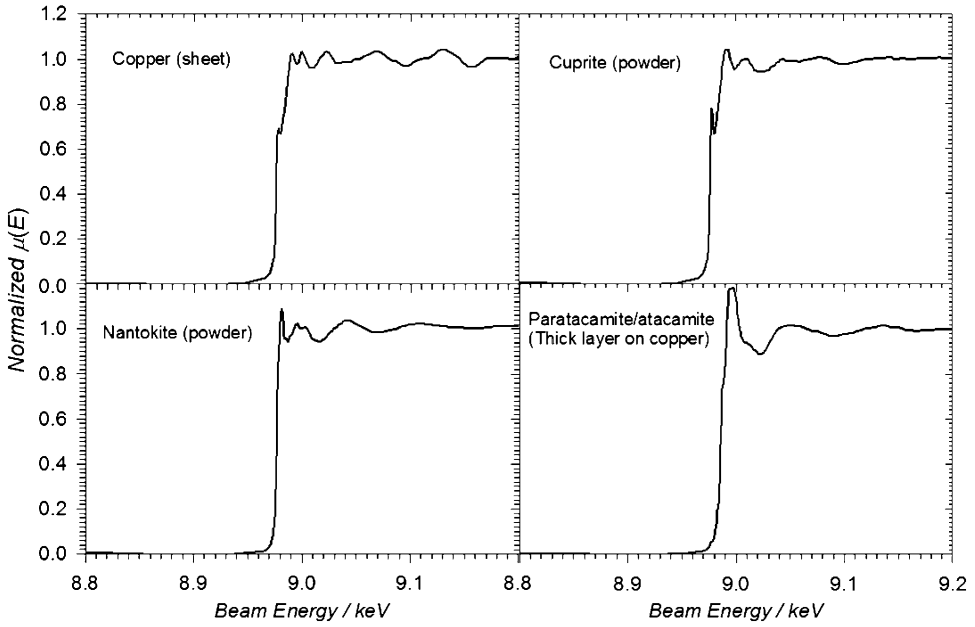


**Figure 2.** Reference spectra gathered in the X-ray fluorescence mode using the DUBBLE beamline.[8]

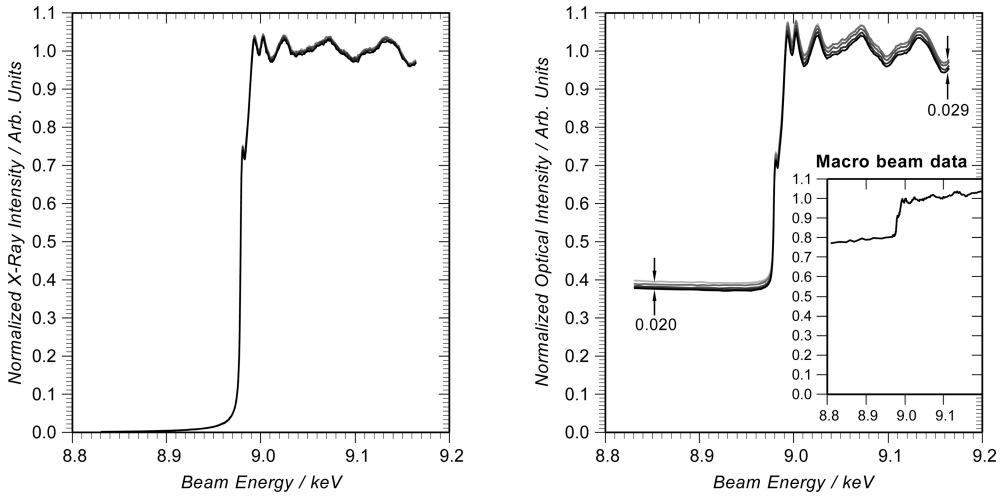


**Figure 3.** Five 10 min scans using an X-ray microbeam to collect K-edge XANES from a polished copper surface. The X-ray fluorescence XANES channel (left) and XEOL-XANES (right) were collected simultaneously. While the XANES is stable (successive scans superimpose), the XEOL-XANES shows a monotonic increase in the pre-edge background and the postedge signal. The geometric similarity of the edge and postedge regions in both types of spectra shows that the pre-edge background in the XEOL-XANES comes from emission channels which turn off at the edge. The inset shows data from the macrobeam where the pre-edge signal is much higher.

not possible with the optics in this proof of concept device. Scan times varied between 5 min and 3 h according to the experiment and were structured similarly to those above, with large monochromator steps in the pre-edge region and smaller steps subsequently. Additive and subtractive dichroic filters (Edmund Optics, U.K., red #52-528, green #52-534, blue #52-531, long pass #47-620, and short pass #47-286); cyan #52-537, magenta #52-540, and yellow #52-543) were used to obtain preliminary information on the spectral content of the XEOL for the macrobeam experiments.

No attempt was made to protect the samples with a gas blanket since the main objective of these experiments was to see whether X-irradiation related damage could be observed on the samples and to what extent realistic time lapse measurements might be made (for example) in a controlled environment with which the surface was reacting.

Processing of the raw data was carried out using our software esaProject 2013.[23] In order to display the data so that relative changes between spectra were preserved, raw spectra were first normalized point-by-point to the beam monitor. Then the mean value of the postedge intensity between 8.990 and 9.165 keV was found separately for the first spectrum in each set of 5 XANES spectra and all five normalized to this. Similarly, the mean value in the same postedge energy range was found for the first XEOL-XANES spectrum in a set, and all the spectra in the set were normalized to it. This process leaves the spectra unchanged in shape compared to the raw data. Standard fitting and normalization techniques were not applied to these spectra because they distort the XEOL-XANES data unacceptably, for reasons discussed below.


dx.doi.org/10.1021/ac401646q | Anal. Chem. 2013, 85, 9556−9563

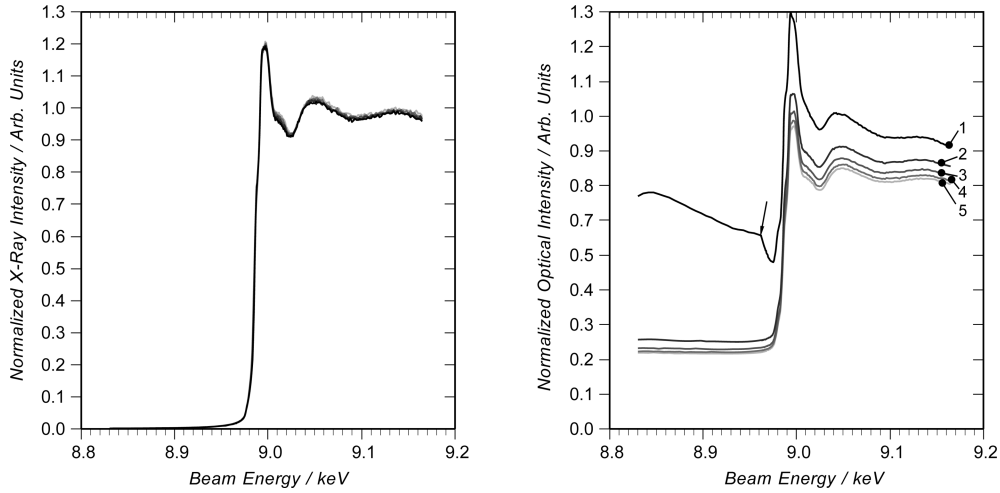


**Figure 4.** Parallel XANES (left) and XEOL-XANES (right) from a thick corrosion layer of copper hydroxychlorides [atacamite and paratacamite, isomers of $Cu_2(OH)_3Cl$) on copper]. The sharp knee in the pre-edge region of scan 1 in the XEOL-XANES (arrowed) occurs where the monochromator stepping rate (eV/s) is reduced.

## RESULTS AND DISCUSSION

Figure 2, for comparison with Figures 3−8, contains reference XANES spectra measured in the X-ray fluorescence mode and gathered under macrobeam conditions. These are plotted conventionally as normalized $\mu(E)$ versus beam energy $E$ and the data collection and processing is described in detail elsewhere.[8]

**Copper.** Figure 3 shows the sequence of 5 XANES and XEOL-XANES spectra collected in parallel from a polished copper surface cleaned with 2-propanol. The main features of both sets of spectra are typical of Cu K-edge XANES. However, whereas the Cu edge rises around 3 orders of magnitude in the XANES data, the XEOL-XANES shows a high level of pre-edge fluorescence in the UV−NIR region sampled. This is a typical difference observed between XANES and XEOL-XANES across all the spectra from the cuprous surfaces reported here and, indeed, spectra from tin, lead, and other materials.

The XANES spectra are identical with one another within the noise. For the XEOL-XANES, there is a rise of 0.02 in the pre-edge fluorescence and 0.029 in the mean post-edge value. The latter is partly accounted for by the increase in background, but there is also a small but significant increase in the height of the Cu edge itself.

The modulation of the XANES spectra is decreased a little by self-absorption in comparison with that of the XEOL-XANES, but there is no sign of an edge shift or structural change with X-ray dose in either case. The surface specificity of XEOL-XANES compared to XANES has been demonstrated elsewhere.[7] In addition, a technique specific to the top nanometer or so, such as ultra low-energy dynamic secondary ion mass spectrometry (uleSIMS), will show these surfaces to be coated with a complex cocktail of organic contaminants and alkali-metal compounds, despite the cleaning in propanol. We therefore attribute a small part of the background fluorescence in the XEOL-XANES to this material, and the increase in the Cu-edge height to its partial breakdown and removal, possibly in reactions with ozone generated by the beam.

A comparison of the first XEOL-XANES scan from the microbeam of I18 with the macrobeam on DUBBLE (inset to Figure 3) gives a pre-edge signal which is 10 times higher on I18, whereas the signal just postedge is 22 times higher. An absolute difference in signal levels (>$10^6$ counts/sec on I18 and >$6 \times 10^4$ counts/sec on DUBBLE) is to be expected because DUBBLE was used with no sagittal focusing, and the ring at ESRF was, in any case, running in 16-bunch mode (around 25% of the current at DLS at that time). However, the fact that the edge height above the pre-edge signal is a factor of >2 higher on I18 suggests that only the end stages of the cleaning process were observed in the scans on I18, implying a far more rapid change in the first few moments of the data taking.

Although we explain a small fraction of the pre-edge signal in the XEOL-XANES from I18 by optical fluorescence from surface contamination, a comparison between the edges in the XANES and XEOL-XANES data shows that most of the pre-edge signal in the latter is due to copper-related radiative processes in the top 100 nm or so, as follows.

The peak due to the interband transition at 8.981 keV occurs at a relative height of 0.7 in both types of spectrum. This means that the XEOL pre-edge signal of 0.4 is not the zero level for the spectrum, otherwise this peak would be at a higher relative intensity in the XEOL data. So, the postedge data are not "sitting on" the pre-edge signal (as, for example, they would be if the optical emission was from a surface contaminant). The pre-edge signal must therefore arise from radiative de-excitation of the ionization of all the Cu L and other outer levels through channels which do not persist at high probability once X-rays are absorbed on the K level (although the end states may be the same).[24,25] This leads to the following problem in data processing: Typically, XANES data might be processed by fitting a spline to the pre-edge region and subtracting this, then normalizing the data to a second spline representing the local mean of the postedge data. Subtracting the high background level from the XEOL-XANES data in a similar way will significantly increase the edge gradient and change the relative position of features on the edge, such as the interband transition at 8.981 keV. Instead, the subtraction process might be replaced by fitting a spline to the lower part of the edge itself (e.g., the region 0.45−0.7 relative intensity in these data) and extrapolating this to zero. Unfortunately, one cannot take this as a blanket approach to all the XEOL-XANES data in this paper, as the background is clearly additive to the spectrum in some cases.


dx.doi.org/10.1021/ac401646q | Anal. Chem. 2013, 85, 9556−9563

**Mixed Hydroxychlorides [Atacamite/Paratacamite–$Cu_2(OH)_3Cl$] on Copper.** Figure 4 shows a similar data set from a layer of mixed atacamite and paratacamite on copper several hundred micrometers thick. Here, the relative proportions of the XANES and XEOL-XANES spectra show that some part of the pre-edge signal in the latter is additive. Again, the XANES data for each scan are superimposed to within the noise level, showing that the are no measurable changes in the bulk of the layer. However, the first XEOL-XANES spectrum shows a rapidly decreasing background with a sharp dip at 8.962 keV where the monochromator step becomes much smaller. Although the measurement time stays the same, the decreased scan rate means that the time taken to scan a given energy range increases more than 10 times. The decrease in signal in the pre-edge region is symptomatic of the destruction of a light-emitting compound on the surface, and the change of slope shows that it is probably a phosphorescent substance that is being destroyed. (The light emission is decaying on a timescale which is long compared to the 1 s acquisition time.) However, the fact that the postedge detail stays the same shape (characteristic of paratacamite) shows that it is not a copper compound which is being lost (but it is possible that the fluorescence of a copper compound is being modified by the X-rays). X-ray diffraction data show that the protocol used to prepare the paratacamite layer leaves behind significant amounts of sodium chloride and sodium nitrate. It is possibly one or both of these that is being destroyed, and the phosphorescence of Cu-doped sodium chloride due to both radiation damage and the doping has been described by others.[26,27] Another possibility is suggested when considering these data in comparison with that from nantokite below. With regard to Figure 4, in the 10 min scan time of the first scan, the XEOL background signal decreases by a factor of 2.8. In the four subsequent scans, the decrease is much less, but the postedge intensity decreases by significantly more than the background. This suggests a shift in the wavelength of the optical emission as the edge is crossed and an increasing effect of either an absorber for this wavelength range or damage to the emitter.

A comparison of data from the red, green, and blue filters (Figure 5), using the macrobeam, shows there is indeed a shift in the wavelength. The data in Figure 5 have been normalized to the mean postedge value of the unfiltered signal. The pre-edge signal is predominantly green (in the range of 500–575 nm), and this also contains the phosphorescent component. Postedge, there is a relative increase in the blue emission (400–500 nm). The white line is characterized by an enhanced emission in the green band, entirely lacking in the blue. The macrobeam signals all show flat pre-edge signals (no damage) but a dip where the scan rate decreases (phosphorescence).

**Nantokite (CuCl) on Copper.** Nantokite is produced on copper through the application of a simple protocol, which involves soaking a clean copper coupon in saturated $CuCl_2$ solution and rinsing the residual $CuCl_2$ away with water. Unfortunately, both this latter process and subsequent exposure to air result in decomposition of the CuCl through fast and slow hydrolization to form cuprite and paratacamite.[23,28]

Figure 6 shows XANES and XEOL-XANES data from a freshly made nantokite layer an hour or so old. The XANES data are entirely characteristic of the underlying copper because the nantokite layer is thin.[7] The XEOL-XANES data show the presence of a mixture of nantokite and paratacamite (compare with reference spectra in Figure 2). In particular, the white line

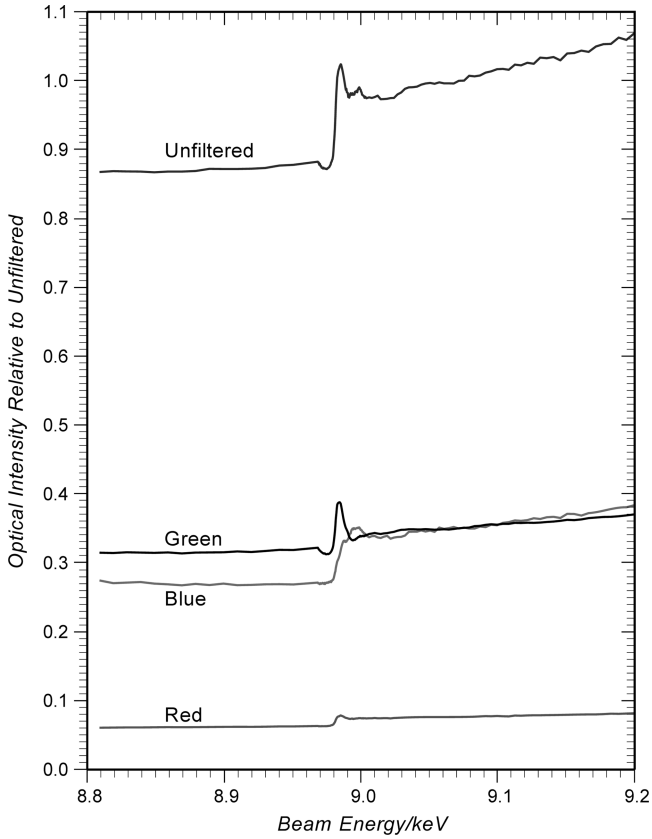


**Figure 5.** XEOL-XANES data from a copper coupon coated with a mixture of atacamite and paratacamite taken using the macrobeam. Three successive scans through red, green, and blue bandpass filters show a significant increase in the blue emission postedge. Data from the other filters mentioned in the text is consistent with this.

observed at 8.986 keV is characteristic of nantokite (arrowed in the left pane of Figure 6). (The term "white line" is used in X-ray absorption spectroscopy to describe a peak occurring more or less at the top of the edge. It comes from the appearance of data recorded by dispersion of transmitted X-rays across a photographic plate in early measurements.) With consideration of the pre-edge region first, the behavior here is similar to that for paratacamite, but there are no sodium compounds involved in the production. Measurements on other nantokite layers aged for several days show significantly less nantokite (and more cuprite and paratacamite) and also around 20% less phosphorescence at the start of the analysis. Other features are identical to those shown here. It therefore seems likely that the rapidly decaying pre-edge signal originates from the nantokite. At the same time, the white line decreases in intensity as the X-ray dose increases, until only the signatures of paratacamite and cuprite remain in the spectrum. Since nantokite reacts readily with oxygen and water vapor in the air, it is not surprising that the power input from the beam, combined with the $O_3$ generation, causes the nantokite to decompose. The macrobeam data (inset) consistently show a rather different spectrum, which we demonstrate elsewhere[7] is characteristic of nantokite. In particular, the white line is more prominent (and remains stable over several hours). It therefore seems that the microbeam has started to decompose the nanotkite early in the first scan.

**Cuprite ($Cu_2O$) on Copper.** The XANES and XEOL-XANES data shown in Figure 7 are characteristic of cuprite[7]


dx.doi.org/10.1021/ac401646q | Anal. Chem. 2013, 85, 9556–9563

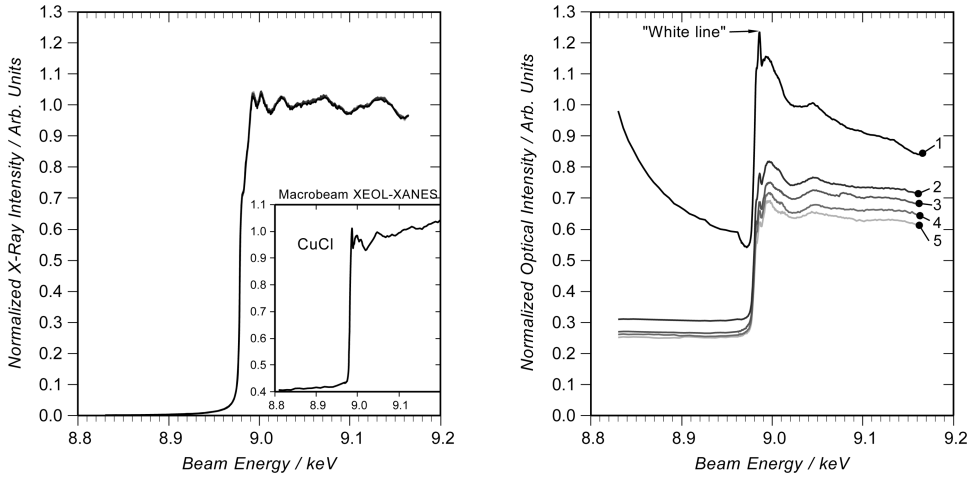


**Figure 6.** Microbeam scans of XANES (left) and XEOL-XANES (right) from nantokite (CuCl)-coated copper with macrobeam XEOL-XANES of nantokite as an inset. The XANES is entirely characteristic of copper because the layer is thin. The macrobeam XEOL-XANES is characteristic of nantokite, and the microbeam XEOL-XANES is loosing a phosphorescent emitter and decomposing to paratacamite under the beam.

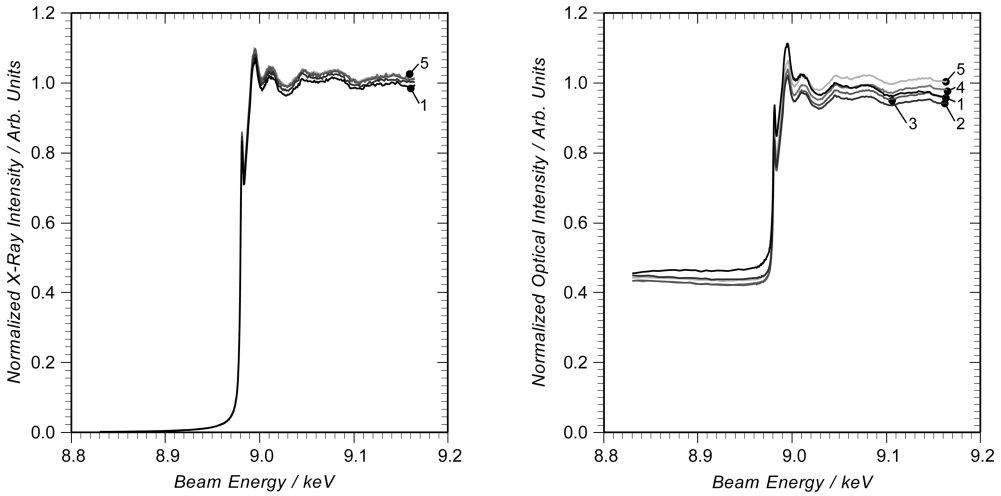


**Figure 7.** Microbeam XANES (left) and XEOL-XANES (right) from cuprite ($Cu_2O$) on copper. As for copper, the edge and postedge regions of both XANES and XEOL-XANES spectrum are geometrically similar, showing that the pre-edge background in the XEOL-XANES is from emitters which turn off at the edge.

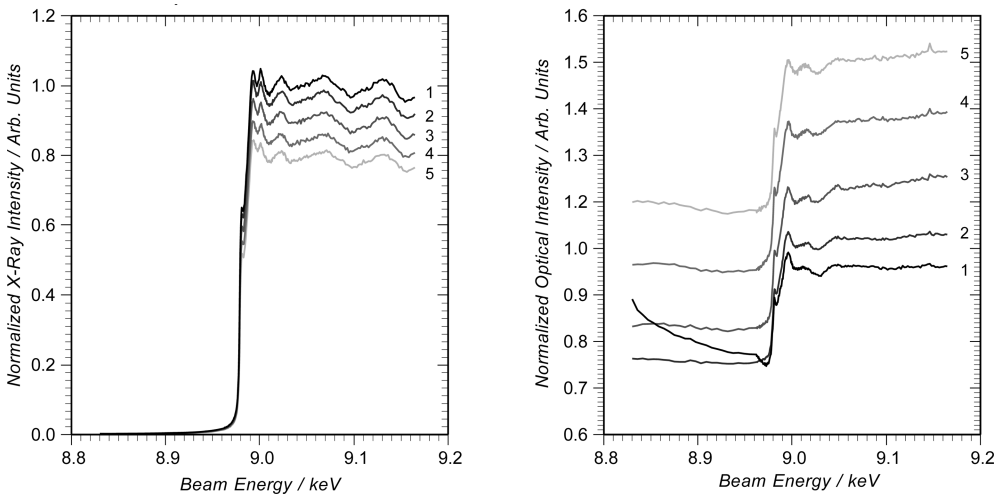


**Figure 8.** Five XANES (left) and XEOL-XANES (right) scans from a thin cuprite layer on lead bronze. The XANES is characteristic of the copper substrate because the layer is thin, but the copper is apparently being covered up during the measurement. Conversely, the background and the edge height on the XEOL-XANES (characteristic of cuprite, cf. Figures 2 and 7) are enhanced.


dx.doi.org/10.1021/ac401646q | *Anal. Chem.* 2013, 85, 9556−9563

with its pronounced interband transition on the edge at 8.982 keV. The geometrical similarity of the edge and postedge regions in both types of spectrum (especially the similar relative positions of the midedge feature) shows that, as for copper, the pre-edge background in the XEOL-XANES comes from emission channels which turn off at the edge. Copper itself does not show any tendency to oxidize in the 50 min of X-ray exposure (Figure 1). On the other hand, preoxidized copper in the form of cuprite was one of the few examples we observed where the XANES showed some variation over time as well as the XEOL-XANES. Figure 7 shows a small increase in the cuprite intensity in XANES over the 5 spectra. However, since the layer is initially thick enough that there is no sign of copper in the first spectrum taken, this cannot be due to an increase in the cuprite thickness. Looking at the XEOL-XANES, we see that there is a 7% decrease in the pre-edge background, between the first and second spectra, with a corresponding decrease in the postedge average. In subsequent scans, the pre-edge level stays similar, while the postedge level increases. This suggests the removal of a fluorescing surface compound, which was absorbing both a fraction of the X-ray fluorescence and a larger fraction of the optical fluorescence from the cuprite. The cuprite is made by immersion of the copper in sodium sulfate solution. The observed behavior is consistent with the decomposition of this by the beam.

**Cuprite ($Cu_2O$) on Lead Bronze.** A more complex example of surface modification is found in the examination of a lead-bronze alloy coated with cuprite. Under the microbeam, this sample showed strongly varying behavior from place to place. In some locations, for example, the 5 XANES spectra overlaid and were characteristic of copper (thin cuprite layer), whereas the XEOL XANES showed high levels of pre-edge fluorescence (rather than phosphorescence), which decreased by a total of 10% in the 50 min, and a noisy edge, and a postedge signal characteristic of mixed copper and cuprite spectra (copper seen through thin or patchy cuprite). Figure 8 shows different behavior. The XANES is characteristic of copper but decreases monotonically from scan-to-scan by 20% overall. The XEOL-XANES is characteristic of cuprite on a high and mostly fluorescent background. This increases scan-to-scan, apart from the destruction of some phosphorescence in scan 1. The height of the copper edge above the background also increases. In this material, the lead and copper phases are partially separated,[29] and the grains are quite large (up to 100 $\mu$m across).

Moreover, we find that macrobeam measurements of XEOL from lead and several of its compounds show high levels of pre-edge fluorescence. The irradiated region in Figure 8 most likely includes both lead and copper grains. Given their respective melting points (Pb = 327.46 °C, Cu = 1084.62 °C), heat capacities (Pb = 26.65 J $mol^{-1}$ $K^{-1}$, Cu = 24.44 J $mol^{-1}$ $K^{-1}$), and enthalpies of fusion (Pb = 4.77 kJ $mol^{-1}$, Cu = 13.26 kJ $mol^{-1}$), it is easy to show that if all the input power from the beam ($10^{11}$–$10^{12}$ 9 keV photons $s^{-1}$) thermalized into a cubic grain 50 $\mu$m on a side, the lead would melt in 0.06 to 0.6 s, and the copper in 0.48 to 4.8 s, nearly 8 times longer. Allowing for heat loss mechanisms, it is not nreasonable to find that the lead melts on a short timescale compared with that of the experiment, whereas the copper does not melt at all. One hypothesis to explain the data is therefore that a nearby lead grain melted and wetted the copper, diminishing the XANES signal. At the same time, cuprite grains (melting point 1232 °C) were floating on, or protruding through, the lead. Then lead, or a lead compound, contributes increasingly to the copper pre-edge signal in the XEOL-XANES, and a small increase in X-ray backscattering from the lead enhances the cuprite yield.

## CONCLUSIONS

For all the surfaces reported here, differences between XANES and XEOL-XANES measurements indicate that a microbeam of sufficient power to acquire chemical images of corroded metal surfaces, also modifies the near surface region. Except for the nantokite system where the evolution of the surface into paratacamite was obvious, the determination of the exact surface changes would require a very considerable amount of work on each system. However, reasonable hypotheses have been advanced to explain the data. The proposed effects range from surface cleaning for bare copper, through dissociation of surface contaminants left by the corrosion protocols, to melting of lead grains in a lead bronze.

Comparison between XANES and XEOL-XANES for the cuprite and copper samples shows that the pre-edge background in the XEOL-XANES comes from emission channels, which are blocked with the onset of K-level ionization. In general, therefore, it would not be correct to subtract the pre-edge level when processing the data because it would artificially increase the edge gradient and distort near-edge features. Extrapolation of the edge function downward would be a better strategy in some, but not all, cases. The XANES data from a reference sample would, in this context, give a useful guide to the XEOL-XANES processing in general.

Because of the rather rapid onset of surface modification observed here, we decided to construct a XEOL-based chemical mapping system with the ability to image using a macroprobe beam (i.e., with the imaging vested in a pixelated detector on microscope optics). In this mode, X-ray fluorescence XANES images cannot easily be collected in parallel. However, the provision of some means to collect the total XANES from the irradiated region (e.g., a PIN diode) is straightforward, and the macroprobe imaging system can, in any case, still be used with a microprobe beam, especially if the light is dispersed over the camera face to prevent saturation (e.g., in the wells of a CCD camera). Better still, a photomultiplier-based detector such as that used here can be provided to operate in parallel. However, a critical fator in determining which imaging system is most appropriate is the ability of the sample to absorb the required power density from the beam without damage.

## AUTHOR INFORMATION

### Corresponding Author

*E-mail: m.g.dowsett@warwick.ac.uk.

### Notes

The authors declare no competing financial interest.

## ACKNOWLEDGMENTS

We thank Diamond Light Source for access to beam line I18 under award SP4051. ODXAS1 was constructed by Derrick Richards (University of Warwick) and EVA Surface Analysis (U.K.). Software control was by Gareth K. Jones and EVA Surface Analysis. The proof of concept instrument ODXAS1 and the eCell were part-funded by the Paul Instrument Fund of the Royal Society (U.K.). The authors acknowledge, with thanks, the financial support from the Research Foundation-Flanders (FWO).

## REFERENCES


(1) Taylor, R. P.; Finch, A. A.; Mosselmans, J. F. W.; Quinn, P. D. *J. Lumin.* **2013**, *134*, 49−85.
(2) Martínez-Criado, G.; Alén, B.; Sans, J. A.; Homs, A.; Kieffer, I.; Tucoulou, R.; Cloetens, P.; Segura-Ruiz, J.; Susini, J.; Yoo, J.; Yi, G. *Nucl. Instrum. Methods Phys. Res.* **2012**, 36−39.
(3) O'Malley, S. M.; Revesz, P.; Kazimirov, A.; Sirenko, A. A. *J. Appl. Phys.* **2011**, *109*, 124906-1−124906-5.
(4) D'Silva, A. P.; Fassel, V. A. *Anal. Chem.* **1977**, *49*, 638−641.
(5) Hayakawa, S.; Hirose, T.; Yan, L.; Morishita, M.; Kuwano, H.; Gohshi, Y. *X-ray Spectrom.* **1999**, *28*, 515−518.
(6) Quinn, F.; Poolton, N.; Malins, A.; Pantos, E.; Andersen, C.; Denby, P.; Dhanak, V.; Miller, G. *J. Synchrotron Radiat.* **2003**, *10*, 461−466.
(7) Dowsett, M. G.; Adriaens, A.; Jones, G. K. C.; Poolton, N.; Fiddy, S.; Nikitenko, S. *Anal. Chem.* **2008**, *80*, 8717−8724.
(8) Adriaens, A.; Dowsett, M. G.; Jones, G. K. C.; Leyssens, K.; Nikitenko, S. J. *Anal. At. Spectrom.* **2009**, *24*, 62−68.
(9) Holroyd, R. A. and Preses, J. M. Radiation Chemical Effects of X-rays on Liquids. In *Chemical Applications of Synchrotron Radiation: X-ray Applications*; Sham, T-K., Ed.; World Scientific: Singapore, 2002; Vol. 2, Chapter 21, pp 987−1008.
(10) Tresmin, A. S.; Pearson, J. F.; Nichols, A. P.; Owens, A.; Brunton, A. N.; Fraser, G. W. *Nucl. Instrum. Methods Phys. Res., Sect. A* **2001**, *459*, 543−551.
(11) Paparazzo, E. *Surf. Sci. Lett.* **1990**, *234*, L253−L258.
(12) Neuhold, A.; Novák, J.; Flesh, H.-G.; Moser, A.; Djuric, T.; Grodd, L.; Grigorian, S.; Pietsch, U.; Resel, R. *Nucl. Instrum. Methods Phys. Res., Sect. B* **2012**, *284*, 64−68.
(13) Ohmori, Y.; Yamaguchi, M.; Yoshino, K.; Inuishi, Y. *Jpn. J. Appl. Phys.* **1997**, *16*, 181−182.
(14) Nygård, K.; Gorelick, S.; Vila-Comamala, J.; Färm, E.; Bergamaschi, A.; Cervellino, A.; Gozzo, F.; Patterson, B. D.; Ritala, M.; David, C. *J. Synchrotron Radiat.* **2010**, *17*, 786−790.
(15) Magorrian, B. G.; Allinson, N. M. *Nucl. Instrum. Meth. in Phys. Res., Sect. A* **1988**, *273*, 599−604.
(16) Owen, R. L.; Yorke, B. A.; Pearson, A. R. *Acta Crystallogr.* **2012**, *D68*, 505−510.
(17) Mosselmans, J. F. W.; Quinn, P. D.; Dent, A. J.; Cavill, S. A.; Moreno, S. D.; Peach, A.; Leicester, P. J.; Keylock, S. J.; Gregory, S. R.; Atkinson, K. D.; Rosell, J. R. *J. Synchrotron Radiat.* **2009**, *16*, 818−824.
(18) Nikitenko, S.; Beale, A. M.; van der Eerden, A. M. J.; Jacques, S. D. M.; Leynaud, O.; O'Brien, M. G.; Detollenaere, D.; Kaptein, R.; Weckhuysen, B. M.; Bras, W. *J. Synchrotron Radiat.* **2008**, *15*, 632−640.
(19) Dowsett, M.; Adriaens, A. *Anal. Chem.* **2006**, *78*, 3360−3365.
(20) Beldjoudi, T.; Bardet, F.; Lacoudre, N.; Andrieu, S.; Adrianes, A.; Constantinides, I.; Brunella, P. *Rev. Metall. (Les Ulis, Fr.)* 2001, September, 803−808.
(21) Lamy, C. *Stabilisation d'Objets Archéologiques Chlorurés en Alliage Cuivreux*; Report ARC'Antique, Nantes, France, 1977.
(22) Adriaens, A.; Dowsett, M. *Acc. Chem. Res.* **2010**, *43*, 927−935.
(23) Dowsett, M. G.; Adriaens, A.; Martin, C.; Bouchenoire, L. *Anal. Chem.* **2012**, *84*, 4866−4872.
(24) Emura, S.; Moriga, T.; Takizawa, J.; Nomura, M.; Bauchspiess, K. R.; Murata, T.; Harada, K.; Maeda, H. *Phys. Rev. B* **1993**, *47*, 6918−6930.
(25) Sparks, C. J. *Phys. Rev. Lett.* **1974**, *33*, 262−265.
(26) Nanto, H.; Endo, F.; Hirai, Y.; Murayama, K.; Nasu, S. *Nucl. Instrum. Meth. in Phys. Res., Sect. B* **1994**, *91*, 205−209.
(27) Hirai, M. *J. Phys. Chem. Solids* **1990**, *7*, 737−745.
(28) Scott, D. A. *Copper and Bronze in Art: Corrosion, Colorants, Conservation*; The Getty Conservation Institute: Los Angeles, 2002.
(29) Constantinides, I.; Gritsch, M.; Adriaens, A.; Hutter, H.; Adams, F. *Anal. Chim. Acta* **2001**, *440*, 189−198.